

Synchronization-desynchronization transitions in networks of circle maps with sinusoidal coupling

Yun Zhai(翟云), Jinghua Xiao(肖井华), and Zhigang Zheng(郑志刚)
Citation: Chin. Phys. B, 2023, 32 (**6**): 060505. DOI: 10.1088/1674-1056/acc062
Journal homepage: http://cpb.iphy.ac.cn; http://iopscience.iop.org/cpb

What follows is a list of articles you may be interested in

Stability and multistability of synchronization in networks of coupled phase oscillators

Yun Zhai(翟云), Xuan Wang(王璇), Jinghua Xiao(肖井华), and Zhigang Zheng(郑志刚)
Chin. Phys. B, 2023, 32 (**6**): 060503. DOI: 10.1088/1674-1056/acc808

Synchronization of stochastic complex networks with time-delayed coupling

Duolan(朵兰), Linying Xiang(项林英), and Guanrong Chen(陈关荣)
Chin. Phys. B, 2023, 32 (**6**): 060502. DOI: 10.1088/1674-1056/acc44e

A novel fractional-order hyperchaotic complex system and its synchronization

Mengxin Jin(金孟鑫), Kehui Sun(孙克辉), and Shaobo He(贺少波)
Chin. Phys. B, 2023, 32 (**6**): 060501. DOI: 10.1088/1674-1056/acc0f6

Diffusive field coupling-induced synchronization between neural circuits under energy balance

Ya Wang(王亚), Guoping Sun(孙国平), and Guodong Ren(任国栋)
Chin. Phys. B, 2023, 32 (**4**): 040504. DOI: 10.1088/1674-1056/ac7bff

Influence of coupling asymmetry on signal amplification in a three-node motif

Xiaoming Liang(梁晓明), Chao Fang(方超), Xiyun Zhang(张希昀), and Huaping Lü(吕华平)
Chin. Phys. B, 2023, 32 (**1**): 010504. DOI: 10.1088/1674-1056/ac9363

Synchronization–desynchronization transitions in networks of circle maps with sinusoidal coupling

Yun Zhai(翟云)[1,2,3], Jinghua Xiao(肖井华)[1], and Zhigang Zheng(郑志刚)[2,3,†]

[1] *School of Science, Beijing University of Posts and Telecommunications, Beijing* 100876, *China*
[2] *Institute of Systems Science, Huaqiao University, Xiamen* 361021, *China*
[3] *College of Information Science and Engineering, Huaqiao University, Xiamen* 361021, *China*

(Received 9 February 2023; revised manuscript received 22 February 2023; accepted manuscript online 2 March 2023)

Coupled phase oscillators are adopted as powerful platforms in studying synchrony behaviors emerged in various systems with rhythmic dynamics. Much attention has been focused on coupled time-continuous oscillators described by differential equations. In this paper, we study the synchronization dynamics of networks of coupled circle maps as the discrete version of the Kuramoto model. Despite of its simplicity in mathematical form, it is found that discreteness may induce many interesting synchronization behaviors. Multiple synchronization and desynchronization transitions of both phases and frequencies are found with varying the coupling among circle-map oscillators. The mechanisms of these transitions are interpreted in terms of the mean-field approach, where collective bifurcation cascades are revealed for coupled circle-map oscillators.

Keywords: synchronization, circle map, Kuramoto model, bifurcation

PACS: 05.45.Xt, 05.45.Ra **DOI:** 10.1088/1674-1056/acc062

1. Introduction

Self organization and collective behaviors can be extensively observed in complex systems, ranging from physics, chemistry, biology to economic and social sciences.[1] A systematic exploration of the emergence of complex systems is the core mission of complexity science.[2]

Synchronization implies the rhythmic coordination between two or more elements, which has been ubiquitously observed and relevant in many processes,[3] ranging from groups of cardiac pacemaker cells,[4] coupled metronomes,[5] large groups of fireflies,[6,7] biochemical oscillators,[8] oscillating neutrinos,[9] power grids[10] and neuronal synchronization.[11] Further studies have been extended to chaotic systems, and complete synchronization,[12,13] generalized synchronization,[14,15] lag synchronization,[16] and even measure synchronization[17] have been exhaustively explored. With the developments of network sciences,[18,19] synchronization dynamics on complex networks have also become a center of interest in relating to collective dynamics, spreading and percolation, and explosive phenomena.[20–23]

A simple pointcut in explorations of synchronization is to model unit dynamics as phase oscillators. Starting from Winfree[24] and Kuramoto,[25] coupled phase oscillators such as the Kuramoto model[26,27] have been adopted as prototype models in exploring synchronization behaviors ubiquitously existing in various backgrounds.

Most of the phase models are described by differential equations, i.e., by adopting the continuous-time dynamics. Maps, i.e., discrete-time dynamics, may exhibit completely different properties in studies of nonlinear dynamics. Such is also the case of the study of synchronization problem. Kaneko *et al.* studied the coupled map lattices and found more complicated while interesting behaviors.[28]

For coupled phase map oscillators, there have been numerous studies on coupled sine-circle maps.[29] It is well known that a single sine-circle map has very complex dynamics including periodic, quasiperiodic, and chaotic behaviors. Circle maps were also applied to explore the existence of high-dimensional quaisperiodicity (torus).[30,31] As a population of sine-circle maps are coupled to each other, the intermingled influences of coupling and mapping nonlinearities will make a clear analysis very difficult.[32–41]

On the other hand, even for an unperturbed circle map, very complicated synchronization–desynchronization dynamics can be found as these simple oscillators are coupled to each other. In this paper, it is our mission to extensively investigate the synchronization dynamics of coupled circle maps. We find that discreteness may induce much more interesting synchronization behaviors. Multiple synchronization and desynchronization transitions of both phases and frequencies are found with varying the coupling which happen at strong couplings among circle-map oscillators. The mechanisms of these transitions are interpreted in terms of the mean-field approach, where collective bifurcation cascades are revealed for the coupled circle-map oscillators.

This paper is arranged as follows. In Section 2, the coupled circle maps with sinusoidal coupling are introduced. In Section 3, we study the synchronization dynamics of two cou-

[†]Corresponding author. E-mail: zgzheng@bnu.edu.cn

© 2023 Chinese Physical Society and IOP Publishing Ltd

pled circle maps. This can be well described by the dynamics of the sine-circle map. In Section 4, we discuss the dynamics of the coupled maps on networks. Multiple synchronization–desynchronization (SD) transitions are revealed. These transitions can be interpreted in the framework of mean-field approach, where the synchronization transition and the instability of synchronous state are disclosed in Section 5. Section 6 presents a concluding remark.

2. Modeling networks of coupled circle maps

Consider a general topology of mutual interactions among oscillators. If one describes the oscillator dynamics only in terms of phase variable θ, the dynamics should be constrained on the $[0,2\pi]$ circle. Suppose a system of N oscillators with phases and nature frequencies $\{\theta_i(t),\omega_i,i=1,2,\ldots,N\}$. Let us study the time-discrete version of the Kuramoto model, i.e., the coupled circle maps.[28,29] The dynamics of a single oscillator described by the circle map can be written as

$$\theta_i^{t+1}=\theta_i^t+\omega_i, \tag{1}$$

where $t=1,2,\ldots$ is the discrete time.

Since the circle map (1) is linear and does not contain nonlinear perturbations, the dynamical feature is thoroughly determined by the commensurability of the natural frequency ω_i. As ω_i is commensurate, i.e., ω_i can be expressed as the ratio of two integers, the motion of the map on the circle is periodic. On the other hand, when ω is irrational (incommensurate), the motion on the circle is ergodic and quasiperiodic.

By taking into account the couplings among N circle maps, the dynamics can be described as

$$\theta_i^{t+1}=\theta_i^t+\omega_i+\frac{K}{k_i+1}\sum_{j=1}^{N}A_{ij}\sin(\theta_j^t-\theta_i^t),\quad i=1,2,\ldots,N. \tag{2}$$

The coupling topology is described by the adjacency matrix $\boldsymbol{A}=(A_{ij})$, $i,j=1,2,\ldots,N$. One usually sets $A_{ij}=A_{ji}=1$ if oscillators i and j are coupled to each other, and $A_{ij}=A_{ji}=0$ otherwise. The diagonal elements A_{ii} are supposed to satisfy the condition $A_{ii}=-\sum_{j\neq i}A_{ij}=-k_i$, where k_i is the degree of the i-th node. The natural frequencies of oscillators $\{\omega_i\}$ are assumed to be heterogeneous and randomly given by the uniform distribution in $[-\Delta,\Delta]$.

Equation (2) is the discrete version of the following Kuramoto model:

$$\dot{\theta}_i=\omega_i+\frac{K}{k_i+1}\sum_{j=1}^{N}A_{ij}\sin(\theta_j-\theta_i),\quad i=1,2,\ldots,N. \tag{3}$$

There have been extensive theoretical studies on the synchronization behaviors of the model (3).[26,27] For the fully connected network case, i.e., $k_i=N-1$, Eq. (3) describes the dynamics of the traditional mean-field Kuramoto model. In the thermodynamics limit $N\to\infty$, statistical description can be introduced to study the collective behavior of model (3). Kuramoto.[42] proposed the self-consistency approach to analytically predict the transition from incoherence to synchronization. It was found that synchrony among oscillators emerges when the coupling strength exceeds the critical value $K_c=2/\pi g(\omega_0)$, i.e., $R=0$ for $K<K_c$, and $R>0$ as $K>K_c$. Here $g(\omega)$ is the distribution of the intrinsic frequency. The dynamics of synchronization transition can also be resorted to the recently proposed Ott–Antonsen ansatz[43,44] and Watanabe–Strogatz transformation,[45–47] which gives rise to the low-dimensional dynamical equations of order parameters and richer non-stationary collective dynamics of coupled oscillators.

In the following discussion, we will perform numerical simulations of system (2) for Erdos–Renyi (ER) random networks and nearest-neighbor regular (NNR) networks to check the influence of network topology on the synchronization. An ER random network can be constructed by setting a linking probability p for a pair of nodes. For NNR networks, the adjacency matrix satisfies $A_{i,i\pm j}=1$ for $j\leq L$ and $A_{i,i\pm j}=0$ for $j>L$, where L is the neighbor distance. It can be easily seen that $k_i=2L$ for the NNR case.

3. Synchronization of two coupled circle maps

We first study the synchronization dynamics of $N=2$ circle-map oscillators. The dynamics is simplified to two coupled maps

$$\theta_{1,2}^{t+1}=\theta_{1,2}^t+\omega_{1,2}+\frac{K}{2}\sin(\theta_{2,1}^t-\theta_{1,2}^t). \tag{4}$$

The average winding number (frequency) of each oscillator is defined as

$$\Omega_i=\lim_{t\to\infty}\frac{\theta_i^t-\theta_i^0}{t-1}. \tag{5}$$

The synchronization of two oscillators is achieved when $\Omega_1=\Omega_2$. We compute the frequency difference $\Delta\Omega=|\Omega_2-\Omega_1|$ to investigate the synchronization dynamics of the coupled circle maps.

In Fig. 1, the difference $\Delta\Omega$ is plotted against the coupling strength K for different mismatch parameters $\Delta=\omega_2-\omega_1$. It can be seen that for small $\Delta=0.2$, 0.5, and 0.75, $\Delta\Omega$ decreases to 0 smoothly with increasing coupling. For larger $\Delta=1.0$, 1,25, 1.5, and 1.75, $\Delta\Omega$ also decreases as the coupling is increased, but some non-smooth steps such as $\Delta\omega/2\pi=1/6$, $1/4$, $1/3$, $1/2$, … can be found. These steps imply a locked difference between the frequencies of two oscillators, and they are never observed in differential phase dynamical systems. In this sense, the traditional synchronized state means the locking

state $\Delta\omega = 0$, which of course is the largest locking step in all possible steps, as shown in Fig. 1. When the natural-frequency mismatch is too large, i.e., for the curve of $\Delta = 2.0$ in Fig. 1, $\Delta\omega$ will be locked to the 2π step instead of the $\Delta\omega = 0$ step.

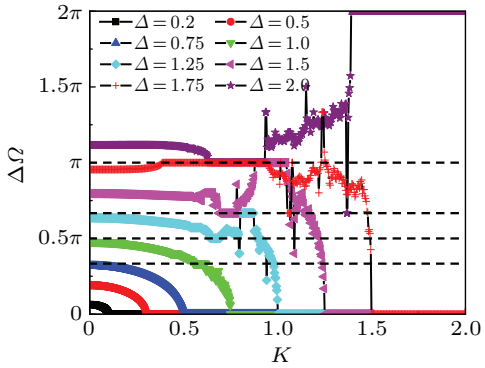


Fig. 1. Synchronization dynamics of $N = 2$ coupled circle maps by plotting the variation of the winding-number difference $\Delta\omega$ with the coupling strength K for different natural-frequency mismatches: $\Delta = 0.2$, 0.5, 0.75, 1.0, 1,25, 1.5, 1.75, and 2.0 (from the bottom up). Several locking staircases such as $\Delta\omega = 0$, $\pi/3$, $\pi/2$, $2\pi/3$, π, ..., and 2π are shown as dashed lines.

It is important to give a thorough understanding of the locking behavior for various parameters. By introducing the phase difference $\phi = \theta_2 - \theta_1$, Eq. (4) can be written as

$$\phi^{t+1} = \phi^t + \Delta - K\sin\phi^t. \tag{6}$$

This is just the so-called sine-circle map, which has been extensively studied[29] in relating to a number of phenomena in driven sustained oscillator, rotator, phase-locked loop, Josephson junction, and cardiac dynamics.[3] The original derivation of the map (6) comes from the physical modeling of periodically driven oscillator, where the mismatch parameter Δ is proportional to the ratio between the period of the driving force T and the period of self-sustained oscillations T_0, i.e., $\Delta = 2\pi T/T_0$. The parameter K is proportional to the amplitude of the external force. For $K = 0$, we have the linear circle map (1), and K governs the nonlinearity level in the map (6).

Different from the driven sustained oscillator, the system we are discussing is composed of two mutually coupled sustained oscillators, and the parameters Δ and K are the difference of the natural frequencies of the two oscillators and the coupling strength, respectively.

In Fig. 2, some typical locking states of $\Delta\Omega = |\Omega_2 - \Omega_1|$ are plotted as a phase diagram on the (K, Δ) parameter plane, where colors correspond to different rational values of $\Delta\Omega/2\pi$ that can be expressed by the ratios of integers m/n. One may readily find that these locking states form the interesting Arnold tongues. This is natural because the locking behavior of the two coupled oscillators is described by Eq. (6). It can be first noted that $0/1$ (red) and $1/1$ (blue) lockings occupy the largest portion of the parameter plane, then $1/2$, $1/3$, $2/3$, ... The measure of these locking tongues decreases with the rationality of the ratio m/n.

A convenient way to present all these locking tongues is to introduce the Farey summation rule, i.e., for two irreducible integer ratios m_1/n_1 and m_2/n_2, a new ratio m/n can be introduced as

$$\frac{m}{n} = \frac{m_1 + m_2}{n_1 + n_2}. \tag{7}$$

If the new ratio m/n is irreducible, then one successfully constructs a new Arnold tongue with a smaller measure than m_1, n_1 and m_2, n_2. The Farey rule gives rise to a Farey tree starting from two seeds $0/1$ and $1/1$. One can also determine the lower boundaries of various locking solutions m/n on the basis of the map (6). All these discussions can be resorted to the results from the sine-circle map. We will not further discuss this topic.

The critical line $K/2\pi = 1$ is labeled in Fig. 2. It should be noted that the map (6) is invertible if $|K/2\pi| \leq 1$, and non-invertible for $|K/2\pi| > 1$. Below the critical line, the dynamics of the sine-circle map is regular (periodic or quasiperiodic), and various Arnold locking tongues do not overlap. When the coupling exceeds the critical value, Arnold tongues begin to overlap with each other, leading to competitions among different resonant lockings and even chaotic dynamics.

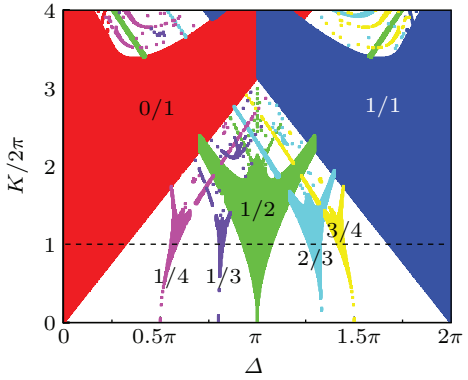


Fig. 2. Phase diagram of the synchronization regimes of $N = 2$ coupled circle maps. Some visible locking tongues are labeled with different colors (from left to right): 0/1 (red), 1/4 (purple), 1/3 (dark purple), 1/2 (green), 2/3 (cyan), 3/4 (yellow), and 1/1 (blue).

4. Synchronization in networks of circle maps

Coupled circle-map systems may exhibit rich and complicated collective dynamics when a population of maps with different individual natural frequencies are coupled to each other. In this section, we discuss the behaviors of coupled circle maps on different network topologies.

First let us distinguish two concepts related to synchrony among oscillators. The first quantity measures the degree of coherence among phases of oscillators, which can be introduced by the following complex order parameter:

$$z(t) = R(t)\,\mathrm{e}^{\mathrm{i}\psi(t)} \equiv \frac{1}{N}\sum_{j=1}^{N}\mathrm{e}^{\mathrm{i}\theta_j^t}, \tag{8}$$

where i is the imaginary unit, $R(t)$ and $\psi(t)$ describe the coherence factor and collective phase, respectively. In the limit

$N \to \infty$, $R = 0$ represents an incoherent state with phases of oscillators homogeneously distributed in $[0, 2\pi)$. $R > 0$ implies some degree of synchrony among oscillators, and $R = 1$ means a fully in-phase synchronous state.

The order parameter $R(t)$ reflects the coherent behaviors of phases of oscillators. One may study the dynamics of $R(t)$ by computing its time average

$$\langle R \rangle = \lim_{T\to\infty} \frac{1}{T} \sum_{t=1}^{T} R(t). \tag{9}$$

The second measure is to describe the degree of frequency locking among oscillators, which can be introduced by the following function:

$$\Delta\Omega = \frac{1}{N} \sum_{j=1}^{N} \left| \Omega_j - \omega_0 \right|, \tag{10}$$

where Ω_j is the time-averaged frequency of the j-th oscillator defined by Eq. (5). Ω_0 is the mean natural frequency of the system

$$\Omega_0 = \frac{1}{N} \sum_{j=1}^{N} \omega_j. \tag{11}$$

All oscillators are frequency locked when $\Delta\Omega = 0$.

The detailed information of the synchronization dynamics can be traced by using the synchronization bifurcation tree $\{\Omega_i(K), i = 1, 2, \ldots, N\}$[48–50] to study the locking processes among oscillators. In the following studies, the number of oscillators is set to be $N = 100$. Natural frequencies of map oscillators obey the uniform distribution in $[-\Delta, \Delta]$, where Δ measures the natural-frequency mismatch.

We first study the collective behaviors of system (2) for different network topologies by computing the relations between $\langle R \rangle$ and the coupling K, which are presented in Fig. 3 for ER random networks and NNR networks containing $N = 100$ oscillator nodes, respectively. The difference $\Delta = 0.1$. For a sparse ER random network with $p = 0.2$, as shown by the square line in Fig. 3, the order parameter experiences a sharp increase at the critical coupling $K^{\rm p}_{\rm c,1} \approx 0.12$. The transition to a large $\langle R \rangle$ implies the emergence of a high degree of phase coherence of oscillators. The order parameter $\langle R \rangle$ continues to increase and approaches $\langle R \rangle = 1$ (full synchrony) with the increase of the coupling K. This strong coherence is maintained for the differential Kuramoto system (3), and $\langle R \rangle \to 1$ as $K \to \infty$. Such is not the fact for coupled circle maps (2). One may find from Fig. 3 that when the coupling K is larger than the second critical value $K^{\rm p}_{\rm c,2} \approx 1.52$, $\langle R \rangle$ begins to decrease with further increasing the coupling K. For the random network with a higher connection probability $p = 0.5$ (circle line), one still finds the synchronous transition at $K \geq K^{\rm p}_{\rm c,1} \approx 0.11$ and the desynchronization transition at $K^{\rm p}_{\rm c,2} \approx 1.67$.

We also investigate synchronization dynamics of coupled circle maps on NNR networks. In Fig. 3, we present the $\langle R \rangle \sim K$ relation for the node degree $k = 10$ (triangle line) and 50 (inverted-triangle line), respectively. It can be seen that the synchronization dynamics on regular networks with different degrees exhibit similar tendency to ER random networks. For $k = 10$, the critical couplings $K^{\rm p}_{\rm c,1} \approx 0.16$, $K^{\rm p}_{\rm c,2} \approx 0.26$. For $k = 50$, $K^{\rm p}_{\rm c,1} \approx 0.14$, and $K_{\rm c,2} \approx 1.66$. As a comparison, $\langle R \rangle$ does not exhibit strong phase coherence and decreases at a much smaller critical value $K_{\rm c,2}$.

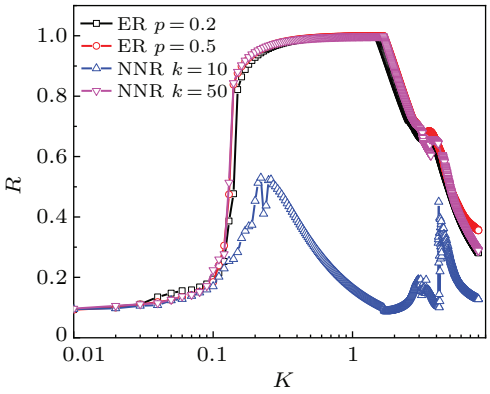


Fig. 3. Synchronization dynamics of coupled circle maps measured by the relations between the order parameter R and the coupling strength K for different network topologies. The number of oscillators is $N = 100$. $\Delta = 0.1$. ER random networks with different connection probabilities: (a) $p = 0.2$, (b) $p = 0.5$. NNR networks with different degrees: (c) $k = 10$, (d) $k = 50$.

We further study the synchronization bifurcation tree presented by the $\{\Omega_i\} \sim K$ profile. These profiles are presented in Figs. 4(a)–4(d) corresponding to the networks discussed in Fig. 3. For convenience, each bifurcation tree is further measured by plotting the difference $\Delta\Omega$ varying with the coupling. To show the details in the small-coupling regime, the K-axis is presented in the logarithm format. It can be clearly found that for all these different cases, oscillators experience complicated clustering processes, i.e., oscillators are frequency locked to form synchronous clusters with increasing coupling, and the clustering dynamics persist until all oscillators are frequency locked to a single cluster at $K \geq K^{\rm f}_{\rm c,1}$. For cases of Figs. 4(a), 4(b) and 4(d), the critical coupling for frequency locking is approximately the same as that for the emergence of phase coherence, i.e., $K \geq K^{\rm f}_{\rm c,1} \approx K^{\rm p}_{\rm c,1}$. This coincidence can be shown and understood from the synchronization bifurcation tree. For ER random networks and NNR networks with large degrees, both long-range shortcut connections for the random networks and enough number of neighbors for the NNR networks ensure a highly efficient frequency locking among oscillators. This gives rise to an explosive-like locking near the critical coupling $K^{\rm f}_{\rm c,1}$, implying a coincidence of frequency locking with phase coherence. For the case presented in Fig. 4(c), $k = 10$, one may still find an intermingled tree structure with multiple

synchrony clusters. In this case, though $\langle R\rangle$ increases drastically at $K^{\rm p}_{\rm c,1}\approx 0.16$, a global frequency locking is not achieved at $K^{\rm p}_{\rm c,1}$ until $K\geq K^{\rm f}_{\rm c,1}\approx 0.27$.

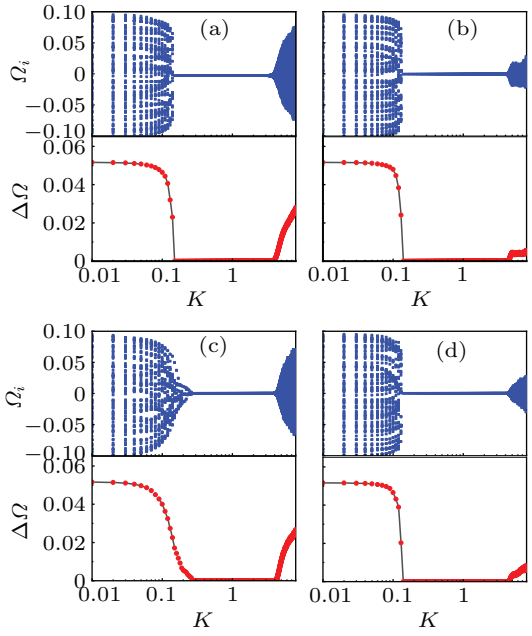


Fig. 4. Synchronization dynamics of $N=100$ coupled circle-map oscillators with the same network topologies as in Figs. 3(a)–3(d). $\Delta=0.1$. For each sub-figure, the upper plot is the synchronization bifurcation tree $\{\Omega_i\}\sim K$, and the lower plot is the frequency difference $\Delta\Omega$ against the coupling strength K.

As one further increases the coupling, the locking states lose their stability as the coupling strength exceeds the second threshold $K^{\rm f}_{\rm c,2}$. It can be seen that frequencies of oscillators $\{\Omega_i\}$ become unlocked when $K>K^{\rm f}_{\rm c,2}$. For the ER network with $p=0.2$, $K^{\rm f}_{\rm c,2}\approx 4.02$, for $p=0.5$, $K^{\rm f}_{\rm c,2}\approx 4.35$. For the NNR network with $k=10$, $K^{\rm f}_{\rm c,2}\approx 4.28$, for $k=50$, $K^{\rm f}_{\rm c,2}\approx 4.6$. As a comparison with the R–K curves presented in Fig. 3, one notices at $K=K^{\rm p}_{\rm c,2}$ that the phase coherence is deteriorated, but the frequency locking is still kept until $K\geq K^{\rm f}_{\rm c,2}>K^{\rm p}_{\rm c,2}$. It is significant to study what happens at $K=K^{\rm p}_{\rm c,2}$ and $K=K^{\rm f}_{\rm c,2}$.

5. Synchronization–desynchronization transitions: mean-field analysis

The above investigations for different network topologies exhibit some common features. We are interested in the transitions from asynchronous to synchronous states and the emergence of desynchronization transition for both phase coherence and frequency locking. It is found that phase and frequency synchronization–desynchronization transitions are different. To understand these transitions, let us study the global coupling case.

The global coupling implies $k_i=N-1$ in Eq. (2), then one obtains

$$\theta_i^{t+1}=\theta_i^t+\omega_i+\frac{K}{N}\sum_{j=1}^{N}\sin\left(\theta_j^t-\theta_i^t\right). \tag{12}$$

In Fig. 5, the synchronization dynamics are exhibited by plotting the variation of the order parameter R [Fig. 5(a)] and the frequency difference $\Delta\Omega$ [Fig. 5(b)] against the coupling strength K for different natural frequency dispersions Δ. One may observe a similar scenario of various transitions between synchronous and asynchronous states. For the global coupling case, the curves become more smooth.

We first analyze the results in Fig. 5(a). There are three branches of the order parameter, and we label them as P-I, P-II, and P-III. The label "P" of these branches implies that they possess different collective states of phases. Branch P-I corresponds to the phase incoherent state for $0\leq K\leq K^{\rm p}_{\rm c,1}$. On this branch, both phases and frequencies of oscillators are not synchronized, and R remains at a small value, $R\sim 1/N$. Branch P-II represents the coherent state for $K^{\rm p}_{\rm c,1}\leq K\leq K^{\rm p}_{\rm c,2}$, where both phases and frequencies are synchronized, i.e., R increases rapidly with increasing the coupling and $R\approx 1$. Branches P-I and P-II are also typical collective states of coupled time-continuous oscillators. As a comparison, the emergence of branch P-III for $K\geq K^{\rm p}_{\rm c,2}$ is much more interesting. On this branch, R decrease with increasing coupling, implying the loss of phase coherence. These three branches experience transitions by changing the coupling. Usually one can observe all these three branches. If Δ is very large , e.g., $\Delta=1.5$, as shown in Fig. 5(a), R directly jumps from branch P-I to P-III in the absence of branch II.

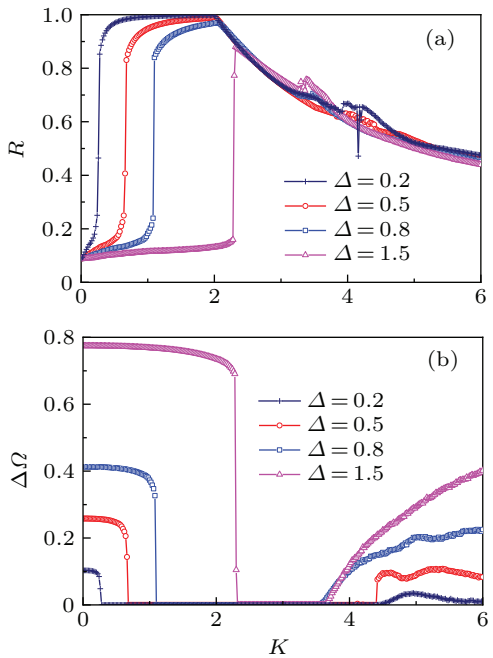


Fig. 5. The synchronization dynamics are exhibited by plotting the variation of the order parameter R and the frequency difference $\Delta\Omega$ against the coupling strength K for different natural frequency dispersions Δ.

As compared to the three branches of the order parameter, in Fig. 5(b), the parameter $\Delta\Omega$ describing frequency synchronization also exhibits three branches. Frequency-unlocking branch F-I exists for $0\leq K<K^{\rm f}_{\rm c,1}$, on which $\Delta\Omega\neq 0$,

where oscillators are not globally synchronized (but some synchronous clusters can be found). When $K \geq K_{c,1}^{f}$, the system becomes globally synchronized, i.e., $\Delta\Omega = 0$, so this state is labeled as branch F-II. Branch F-II ends when $K \geq K_{c,2}^{f}$, which is replaced by branch F-III. On F-III, again one has $\Delta\Omega \neq 0$, indicating that oscillators are no longer frequency locked. This state can also be well demonstrated by the synchronization bifurcation tree in Fig. 4, where the frequencies of oscillators become different from each other at very strong coupling. Similar to the discussions for complex networks, one also notices that $K_{c,1}^{p} \approx K_{c,1}^{p}$ while $K_{c,2}^{p} < K_{c,2}^{p}$.

5.1. Synchronization transition

It is interesting from numerical simulations for different network topologies (ER, NNR, and globally connected) one always observes the above macroscopic states including P-I, P-II, P-III and F-I, F-II, F-III. It is important to understand the physical mechanisms for the transitions among these different states. The synchronization transition can be analytically treated by using the mean-field and self-consistency approach. By using the order parameter (8), Eq. (12) is transformed to

$$\theta_i^{t+1} = \theta_i^t + \omega_i - KR\sin(\theta_i^t - \Theta). \tag{13}$$

In terms of the translational transformation $\theta_i - \Theta \to \theta_i$, Eq. (13) becomes

$$\theta_i^{t+1} = \theta_i^t + \omega_i - KR\sin\theta_i^t. \tag{14}$$

It is interesting that this map is just the standard sine-circle map, where the nonlinear parameter KR is closely related to the order parameter. This means that each oscillator is driven by the mean-field force $KR\sin\theta_i^t$.

Equation (14) can be rewritten by defining the discrete-time derivative $D_t\theta = \theta^{t+1} - \theta^t$ as

$$D_t\theta_i^t = f(\theta_i^t) = \omega_i - KR\sin\theta_i^t. \tag{15}$$

We are interested in the fully synchronized state where all oscillators with the same frequency. According to Eq. (14), the synchronous state of all oscillators implies $\Delta\Omega = 0$, i.e., the globally synchronized state should be the fixed-point solution of Eq. (15) satisfying $D_t\theta_i^t = 0$, leading to

$$\sin\theta_i^* = \frac{\omega_i}{KR}. \tag{16}$$

Then the stationary states satisfy

$$\theta_i^* = \arcsin\left(\frac{\omega_i}{KR}\right), \quad i = 1,2,\ldots,N. \tag{17}$$

Depending on different winding numbers ω_i, an oscillator evolves to the fixed-point solution θ_i^* when $KR \geq \omega_i$, which is stable when

$$f'(\theta_i) = -KR\cos\theta_i^* < 0. \tag{18}$$

This leads to the requirement $\cos\theta_i^* > 0$. This in fact corresponds to the $\Omega = 0/1$ Arnold tongue and is shown in Fig. 6. The critical line of the synchrony tongue is $K_c^i R = \pm\omega_i$. An oscillator with the natural frequency ω_i falls in the synchrony tongue and can be frequency locked when the coupling $K \geq K_c^i = |\omega_i/R|$. This gives the critical coupling for the global frequency locking as

$$K_{c,1}^{f} = \max\{|\omega_i|/R\}. \tag{19}$$

All oscillators will be synchronized when $K \geq K_{c,1}^{f}$. However, since the expression of $K_{c,1}^{f}$ contains the order parameter R, one should determine R. This can be solved in terms of the self-consistency approach.

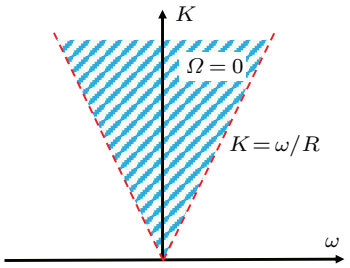


Fig. 6. The critical lines (red dashed lines) and synchronization regime (shaded region) of globally coupled circle-map oscillators. An oscillator can be frequency locked as its natural frequency and the coupling falls in the synchrony tongue.

Now we discuss the transition to phase coherence by using the self-consistency approach. In thermodynamic limit $N \to \infty$, one may introduce the natural-frequency distribution as $g(\omega)$ and the phase distribution for a given ω as $P(\omega;\theta,t)$. The phase distribution function satisfies the following discrete-time continuity equation:

$$D_t P(\omega;\theta,t) = -\frac{\partial}{\partial\theta}\{(\omega - KR\sin\theta)P(\omega;\theta,t)\}. \tag{20}$$

The stationary state satisfies $D_t P(\omega;\theta,t) = 0$. From Eq. (20), one obtains the asynchronous solution

$$P_a(\omega;\theta) = \frac{C}{|\omega - KR\sin\theta|} \tag{21}$$

for $|\omega| \geq KR$, and the synchronous solution

$$P_s(\omega;\theta) = \delta[\theta - \arcsin(\omega/KR)] \tag{22}$$

for $|\omega| \leq KR$. The constant C is the normalization coefficient.

Because all oscillators are considered as synchronous and asynchronous groups, the general distribution is

$$P(\omega;\theta) = P_s(\omega;\theta) + P_a(\omega;\theta). \tag{23}$$

The order parameter defined by Eq. (8) can be written as the following integral:

$$R = \int_0^{2\pi} e^{i\theta} P(\omega;\theta) g(\omega)\,d\omega\,d\theta. \tag{24}$$

Inserting Eq. (23) into the integral, the asynchronous part has no contribution to the order parameter due to the periodicity of $P_{\rm a}$. Then one obtains

$$R = \int_{-\pi/2}^{\pi/2} {\rm e}^{{\rm i}\theta} KR\cos\theta g(\Omega + KR\sin\theta)\,{\rm d}\theta. \tag{25}$$

One has the real part

$$R = KR\int_{-\pi/2}^{\pi/2} \cos^2\theta g(\Omega + KR\sin\theta)\,{\rm d}\theta, \tag{26}$$

and the imaginary part

$$0 = KR\int_{-\pi/2}^{\pi/2} \cos\theta\sin\theta g(\Omega + KR\sin\theta)\,{\rm d}\theta. \tag{27}$$

At the synchronization transition point $K_{\rm c,1}^{\rm p}$, $R \ll 1$, $g(\Omega + KR\sin\theta) \approx g(\Omega) + g''(\Omega)(KR\sin\theta)^2 + \cdots$. By keeping only the first term, Eq. (26) can be integrated out as $K_{\rm c,1}^{\rm p}\pi g(\Omega)/2 = 1$. The critical coupling is

$$K_{\rm c,1}^{\rm p} = \frac{2}{\pi g(\Omega)}. \tag{28}$$

For the homogeneous distribution $g(\omega) = 1/(2\Delta)$, the critical coupling $K_{\rm c,1}^{\rm p} = 4\Delta/\pi$. In Fig. 5, for $\Delta = 0.2$ and 0.5, $K_{\rm c,1}^{\rm p} \approx 0.25$ and 0.56, which agrees well with analytical predictions.

5.2. Instability of synchronous state

The crossover from branch P-II to P-III occurs at a critical value $K_{\rm c,2}^{\rm p}$ signifying some degree of decoherence of phases, although the frequencies of oscillators are still locked ($\Delta\Omega = 0$). It is interesting to understand the mechanism of this crossover. This in fact can be understood as the phase instability of the synchronous state.

The synchronous state corresponds to the period-1 state of the sine-circle map Eq. (14). Phase instability means the instability of period-1 solution. The Jacobian $|1 - KR\cos\theta^*| \leq 1$ leads to

$$0 \leq KR\cos\theta^* \leq 2. \tag{29}$$

By inserting the period-1 solution (17) one obtains $(KR)^2 \leq \omega^2 + 4$. When $(KR)^2 \geq \omega^2 + 4$, the stationary phase state $\{\theta^*\}$ becomes unstable. By considering the minimum frequency $|\omega| = 0$, one obtains the critical condition

$$KR \geq 2. \tag{30}$$

In Fig. 7, the relation between KR and the coupling K is plotted for different Δ. It can be clearly found that the critical couplings $K_{\rm c,2}^{\rm p}$ for the curves passing through the threshold $KR = 2$ agree very well with the turning points of R shown in Fig. 5. For the uniform natural-frequency distribution, the order parameter for the phase synchronous state $R \approx 1$. Therefore for small Δ, when $K \geq K_{\rm c,2}^{\rm p} \approx 2$, the phase synchronous state becomes unstable. This is also in agreement with the critical couplings $K_{\rm c,2}^{\rm p}$ for small $\Delta = 0.2$, 0.5, and even 0.8.

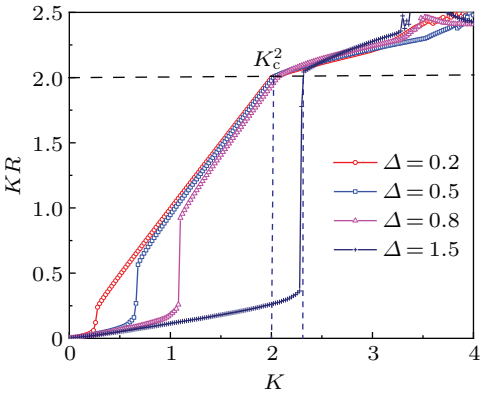


Fig. 7. The variation of KR against the coupling strength K for different $\Delta = 0.2$, 0.5, 0.8, and 1.5. Oscillator number $N = 100$. The threshold curve $KR = 2$ is shown as dashed line.

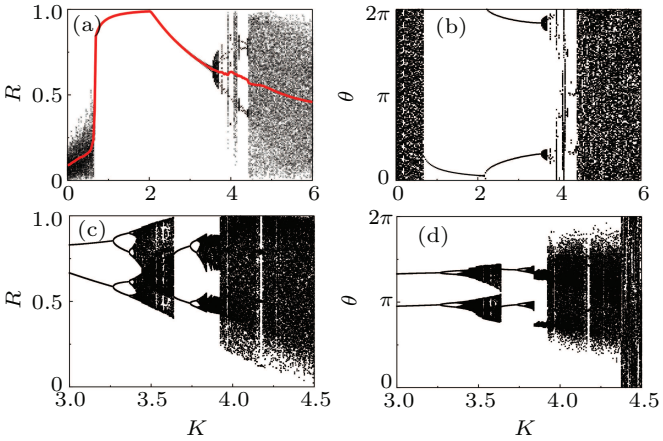


Fig. 8. The bifurcation diagram of (a) the order parameter $R(t)$ and (b) the phase of the oscillator θ_1^t against the coupling strength. Here $N = 100$, $\Delta = 0.2$. In (a), the average $\langle R\rangle$ is plotted in red line as the reference. (c) An enlargement of the bifurcation diagram (a) for $K \in [3.0, 4.5]$. (d) An enlargement of the bifurcation diagram (b) for $K \in [3.0, 4.5]$.

In Fig. 8(a), the bifurcation diagram of the order parameter $R(t)$ is given for $\Delta = 0.2$. To make a comparison, the variation of the averaged order parameter $\langle R\rangle$ is also plotted. It can be found that at the crossover coupling $K_{\rm c,2}^{\rm p}$, $R(t)$ experiences a period-doubling bifurcation, i.e., the synchronized fixed point is replaced by a period-2 state, i.e., an oscillatory behavior of the order parameter. This is a collective period-2 bifurcation originated from the mutual couplings among oscillators. Of course, the period-2 bifurcation can also be well traced by observing microscopic dynamics of one of the oscillators, as shown in Fig. 8(b) by plotting θ_1^t versus the coupling. The period-doubling process does not end at period-2 with the increase of coupling. Figures 8(c) and 8(d) show an enlarged bifurcation diagram of the order parameter $R(t)$ and the phase θ_1^t against the coupling K, respectively. Successive period-doubling bifurcations from period-2 to period-4 and other period-2^m states can be observed. This process

naturally accumulates to the chaotic oscillation of $R(t)$ and θ_i^t. Period windows also reveal intricate collective temporal behaviors of the coupled circle maps.

The bifurcation to period-2 at $K_{c,1}^{p}$ is closely related to the decrease of the averaged order parameter $\langle R \rangle$ with increasing K. In fact, this is a typical transition from a stationary coherence to an oscillatory coherence. The emergence of period doubling also indicates that the single cluster of oscillators splits into two clusters. In Fig. 9, the snapshots of $N = 100$ oscillators at $t = 10^4$ for different couplings are recorded by plotting $\{(\cos\theta_i, \sin\theta_i)\}$. For a weak coupling, as seen from Fig. 9(a) for $K = 0.5$, oscillators are randomly distributed on the unit circle. Correspondingly, $R \approx 0$. When $K > K_{c,1}^{p}$, as shown in Fig. 9(b) for $K = 1.5$, all oscillators are locked to a single compact phase cluster, and $R \approx 1$. Figure 9(c) gives the snapshot for $K = 2.5 > K_{c,2}^{p}$. It is shown that the single cluster in (b) is divided into two phase clusters. It is not difficult from the definition of R in (reforder) that this division leads to the downgrade of R with increasing K. Moreover, each compact part of two clusters becomes dispersed with further increasing K [see Fig. 9(d) for $K = 3.5$], and two parts are eventually merged into a single highly-dispersed cluster, as shown in Fig. 9(e) for $K = 4.0$. This cascade of instability leads to the destruction of the coherence of phases. For very strong coupling exceeding the threshold $K_{c,2}^{f}$, as shown in Fig. 9(f) for $K = 5.0$, frequency locking of oscillators becomes unstable, thus the system evolves in an incoherent manner. The loss of frequency locking for very strong couplings is due to the high-nonlinearity induced chaos and crisis,[51] which enhance the diffusivity of phases and lead to locking instability.

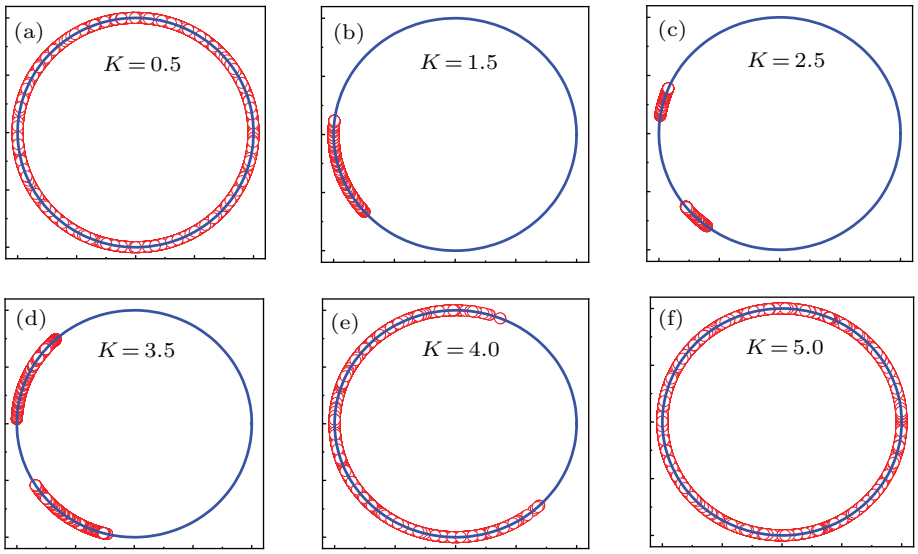


Fig. 9. (a)–(f) Snapshots $(\cos\theta_i, \sin\theta_i)$ of $N = 100$ circle-map oscillators at different coupling strength $K = 0.5$, 1.5, 2.5, 3.5, 4.0, and 5.0.

6. Concluding remarks

In this paper, we focus on the synchronization dynamics of coupled circle-map oscillators, which can be considered as the discrete version of the Kuramoto model. Different from the differential version of the Kuramoto model, the coupled circle-map system exhibits much more complicated synchronization and desynchronization dynamics. Even for two coupled circle maps, complicated synchronization dynamics can be observed, which is related to the Arnold-locking-tongue dynamics of the sine-circle map. Coupled circle maps on different networks exhibit interesting synchronous transition and instability of synchronization, wherever different scenarios for phase coherence and frequency locking are found.

These scenarios can be analytically revealed by studying the mean-field circle map system. In terms of self-consistency approach and stability analysis, the critical couplings for these transitions are given, and the dynamical mechanism of the emergence and instability of synchronous states are revealed. The synchronization behavior of coupled circle maps indicates a distinct difference between differential dynamics and discrete-time mappings.

It should be noted that the mean-field treatment in dealing with the synchronization transitions can give analytical predictions for the thresholds for these transitions. Moreover, the mean-field sine-circle map can explain the mechanism responsible for the transitions to the loss of phase coherence and the loss of frequency locking. For different network topologies, these transition thresholds are different. In these cases, the mean-field scenario cannot present analytical results.

In fact, the studies of the transitions between incoherence and coherence are very interesting topics. In recent years, there have been numerous studies of Kuramoto model with many different variations, such as weighted coupling,[52–54] nonlinear coupling,[55] high-order coupling,[56] and simplical topologies.[57] Co-existences of ordered, partially ordered, and disordered states lead to rich and complicated collective be-

haviors, e.g., chimera state,[58] explosive synchronization,[59] and so on. By considering different types of coupling mechanisms, richer behaviors of synchronization–desynchronization transitions can be observed. We believe our study in this paper will arouse more extensive investigations of synchronization transitions in coupled nonlinear oscillator systems.

Acknowledgement

Project supported by the National Natural Science Foundation of China (Grant No. 11875135).

References

[1] Auyang S Y 1998 *Foundations of complex-system theories: In economics, evolutionary biology, and statistical physics* (Cambridge: Cambridge University Press)
[2] Zheng Z G 2021 *An introduction to emergence dynamics in complex systems* (Singapore: Springer Singapore) pp. 133–196
[3] Pikovsky A, Rosenblum M and Kurths J 2001 *Synchronization: a universal concept in nonlinear sciences* (Cambridge: Cambridge University Press)
[4] Osaka M 2017 *Appl. Math. B* **8** 1227
[5] Jia J, Song Z W, Liu W Q, Kurths J and Xiao J 2015 *Sci. Rep.* **5** e0118986
[6] Ermentrout B 1991 *J. Math. Biol.* **29** 571
[7] Buck J B and Buck E 1968 *Science* **159** 1319
[8] Kiss I Z, Zhai Y and Hudson J L 2002 *Science* **296** 1676
[9] Pantaleone J 1998 *Phys. Rev. D* **58** 073002
[10] Witthaut D, Hellmann F, Kurths J, Kettemann S, Meyer-Ortmanns H and Timme M 2022 *Rev. Mod. Phys.* **94** 015005
[11] Bick C, Goodfellow M, Laing C R and Martens E A 2020 *J. Math. Neurosci.* **10** 9
[12] Pecora L M and Carroll T L 1990 *Phys. Rev. Lett.* **64** 821
[13] Yang J Z, Hu G and Xiao J H 1998 *Phys. Rev. Lett.* **80** 496
[14] Rulkov N F, Sushchik M M, Tsimring L S and Abarbanel H D I 1995 *Phys. Rev. E* **51** 980
[15] Zheng Z G and Hu G 2000 *Phys. Rev. E* **62** 7882
[16] Rosenblum M G, Pikovsky A S and Kurths J 1997 *Phys. Rev. Lett.* **78** 4193
[17] Hampton A and Zanette D H 1999 *Phys. Rev. Lett.* **83** 2179
[18] Albert R and Barabasi A -L 2002 *Rev. Mod. Phys.* **74** 47
[19] Dorogovtsev S N and Mendes J F F 2022 *The nature of complex networks* (OUP Oxford)
[20] Wang X F 2002 *Int. J. Bifurc. Chaos* **12** 885
[21] Boccaletti S, Latora V, Moreno Y, Chavez M and Hwang D U 2006 *Phys. Rep.* **424** 175
[22] Arenas A, Daz-Guilera A, Kurths J, Moreno Y and Zhou C 2008 *Phys. Rep.* **469** 93
[23] Boccaletti S, Almendral J A, Guan S, Leyva I, Liu Z, Sendiña-Nadal I, Wang Z and Zou Y 2016 *Phys. Rep.* **660** 1
[24] Winfree A T 1967 *J. Theor. Biol.* **16** 15
[25] Kuramoto Y 1975 in *International Symposium on Mathematical Problems in Theoretical Physics*, edited by H. Araki (Berlin, Heidelberg: Springer Berlin Heidelberg) pp. 420–422
[26] Acebron J A, Bonilla L L, Perez Vicente C J, Ritort F and Spigler R 2005 *Rev. Mod. Phys.* **77** 137
[27] Rodrigues F A, Peron T K D M, Ji P and Kurths J 2016 *Phys. Rep.* **610** 1
[28] Kaneko K 1991 *Physica D* **54** 5
[29] Jensen M H, Bak P and Bohr T 1983 *Phys. Rev. Lett.* **50** 1637
[30] Grebogi C, Ott E and Yorke J A 1983 *Phys. Rev. Lett.* **51** 339
[31] Grebogi C, Ott E and Yorke J A 1985 *Physica D* **15** 354
[32] Bauer M and Martienssen W 1991 *Network: Computation In Neural Systems* **2** 345
[33] Chatterjee and Gupte 1996 *Phys. Rev. E* **53** 4457
[34] Qin W X 2001 *Int. J. Bifurc. Chaos* **11** 2245
[35] Osipov G V and Kurths J 2002 *Phys. Rev. E* **65** 016216
[36] Janaki T M, Sinha S and Gupte N 2003 *Phys. Rev. E* **67** 056218
[37] Woo S J, Lee J and Lee K J 2003 *Phys. Rev. E* **68** 016208
[38] Sonawane A R 2010 *Phys. Rev. E* **81** 056206
[39] Das A and Gupte N 2013 *Phys. Rev. E* **87** 042906
[40] Yamagishi J F and Kaneko K 2020 *Phys. Rev. Res.* **2** 023044
[41] Sélley F M and Tanzi M 2021 *J. Stat. Phys.* **189** 05618
[42] Kuramoto Y 1984 *Prog. Theor. Phys.* **71** 1182
[43] Ott E and Antonsen T M 2008 *Chaos* **18** 037113
[44] Ott E and Antonsen T M 2009 *Chaos* **19** 023117
[45] Watanabe S and Strogatz S H 1993 *Phys. Rev. Lett.* **70** 2391
[46] Watanabe S and Strogatz S H 1994 *Physica D* **74** 197
[47] Marvel S A, Mirollo R and Strogatz S H 2009 *Chaos* **19** 043104
[48] Zheng Z G, Hu G, and Hu B B 1998 *Phys. Rev. Lett.* **81** 5318
[49] Zheng Z G, Hu B B, and Hu G 2000 *Phys. Rev. E* **62** 402
[50] Hu B B and Zheng Z G 2000 *Int. J. Bifurc. Chaos* **10** 2399
[51] Zheng Z G 2002 *Commun. Theor. Phys.* **37** 557
[52] Xu C, Gao J, Xiang H R, Jia W J, Guan S G and Zheng Z G 2016 *Phys. Rev. E* **94** 062204
[53] Xu C, Sun Y T, Gao J, Qiu T, Zheng Z G and Guan S G 2016 *Sci. Rep.* **6** 21926
[54] Xu C, Boccaletti S, Guan S G and Zheng Z G 2018 *Phys. Rev. E* **98** 050202
[55] Cai Z K, Zheng Z G and Xu C 2022 *Commun. Nonlinear Sci. Numer. Simul.* **107** 106129
[56] Xu C, Xiang H R, Gao J and Zheng Z G 2016 *Sci. Rep.* **6** 31133
[57] Wang X, Zheng Z G and Xu C 2021 *Phys. Rev. E* **104** 054208
[58] Abrams D M and Strogatz S H 2004 *Phys. Rev. Lett.* **93** 174102
[59] Gómez-Gardeñes J, Gómez S, Arenas A and Moreno Y 2011 *Phys. Rev. Lett.* **106** 128701